

THE 1963 VAJONT LANDSLIDE ANALYSED THROUGH NUMERICAL MODELLING

FILIPPO ZANIBONI, MARIA A. PAPARO & STEFANO TINTI

Università di Bologna - Dipartimento di Fisica e Astronomia - Bologna, Italy

ABSTRACT

The use of numerical modelling to simulate natural phenomena is increasingly widespread, mainly owing to computational capacity improving that makes it possible to face the complexity of the modelling techniques. The 1963 Vajont landslide represents a very interesting case study. The abundance of available data, before and after the event, allows the reconstruction of the initial and final mass morphology. Moreover, the mass compactness and the sudden velocity increase, as inferred from post-event observations and analyses, suggests the existence of a well-defined rupture surface, made of exposed clay layers on the western side of the detachment niche, also under the final deposit. Furthermore, the very high velocity attained by the sliding mass (presumably 20-25 m/s) is a hint for very low values of the bottom friction coefficient, considerably smaller than the usual value for clay material.

In this work we apply to simulate the Vajont landslide an in-house built numerical code, UBO-BLOCK1, based on a Lagrangian approach: the sliding mass is split into several along-a-line interacting blocks, volume conserving and shape changing, and the motion of each block is computed numerically. This allows us to simulate the whole dynamics of the slide and to use observables (mainly the final deposit mass distribution) to constrain the parameter of the model, the most influential of which is the bottom friction coefficient. The main result of our analysis is that, if it is assumed that the west- and the east-side of the

slide move on a sliding surface with a different shape, as suggested in the literature, then the corresponding bottom friction coefficients result to be quite different from one another, which in turn demands an explanation in terms of lithological difference of the contact between the slide and the underlying rock body.

KEY WORDS: landslide, numerical modelling, Lagrangian approach, bottom friction coefficient

INTRODUCTION

The Vajont landslide is a very well-known natural disaster that occurred in 1963 and destroyed Longarone together with some other nearby villages in north-east Italy: the water, displaced by the mass collapsing into the Vajont reservoir and mostly channelled westward into the Piave River valley (see Fig. 1), caused over 2000 casualties. A lot of controversies, of legal, technical and scientific character, started soon to understand the responsibilities of the power plant managers and the features of the catastrophe.

The Mt. Toc flank, which forms the southern side of the basin, was under monitoring even before the slide occurrence, due to some facts suggesting the possibility of a slope failure, difficult however to quantify (MÜLLER, 1964 and 1968). After the event very accurate reconstructions and studies were made, characterizing the mass deposit, the surface of rupture and some aspects of the slide motion (e.g. SELLI & TREVISAN, 1964; CARLONI & MAZZANTI, 1964).

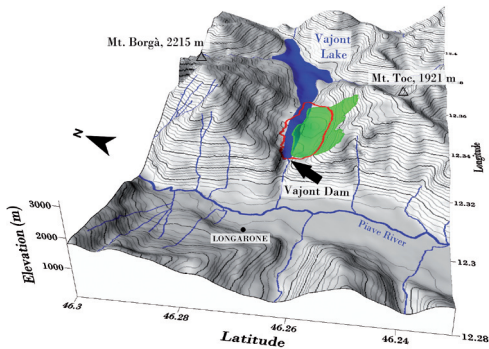


Fig. 1 - Map of the 1963 slide detaching from Mt. Toc flank and collapsing into the Vajont Lake. Initial mass in green, final deposit boundary in red, pre-slide water basin extent in blue

Further contributions came from CALOI (1966), who estimated a slide velocity of around 20 m/s basing on seismic records, and from HENDRON & PATTON (1985), who collated all the preceding studies and data and got confirmation of previous findings: in particular, that 1) the slide moved over well-defined clay layers (exposed in the upper part of the sliding surface), and 2) the mass speed passed suddenly from a few cm/day to tens of m/s, which justifies also why it remained compact with almost undisturbed layers as is still visible in the final deposit.

Many studies concentrated on the friction coefficient μ characterizing such sliding surface. The usual value for the clay (friction angle 17° - 22° , corresponding to $\mu = 0.3$ - 0.4) seemed too high to account for the large velocity reached. CIABATTI (1964), basing only on dynamics considerations, estimated a value of 0.236 for that parameter. Further studies (GHIROTTI, 1994; SEMENZA & GHIROTTI, 1998; TIKA & HUTCHINSON, 1999; SEMENZA, 2000; VARDOLAKIS, 2002; CECINATO *et alii*, 2011) substantially lowered it down to $\mu = 0.07$ - 0.09 invoking auxiliary concurrent processes, such as for instance the pore water pressure increase, due to the heat generated during the slide motion.

Numerical simulations of the landslide and its consequences were the last to appear in the literature of the Vajont case. The recent works by PANIZZO *et alii* (2005) and by BOSA & PETTI (2011) dealt with the water displaced by the slide impacting the Vajont lake. WARD & DAY (2011) applied their model, where the slide mass and the water basin are seen as an ensemble of a great number of particles interacting together.

In this work, following and complementing previ-

ous studies on the Mt Toc slope stability (PAPARO *et alii*, 2013) and on the Vajont landslide simulations carried out by two of the authors (TINTI & ZANIBONI, 2004; ZANIBONI, 2004; ZANIBONI & TINTI, 2013), we concentrate on the analyses of the bottom friction coefficient that was found to be heterogeneous on the slide surface, with higher values on the eastern side and lower on the west. In this paper we will briefly outline the main features of the in-house developed numerical code, UBO-BLOCK1, that was used for the 1963 Vajont landslide simulation; then we will describe the reconstruction of the sliding surface morphology and of the initial and final slide deposit; eventually we will discuss the results of the numerical simulations showing the need of different basal friction coefficients to best fit the available data.

NUMERICAL MODEL

Complex phenomena like landslides need a lot of simplifications to be simulated, that however have to catch all essential aspects of the involved physical processes to provide meaningful results. Keeping this in mind the code UBO-BLOCK1, developed by the University of Bologna Tsunami Research Team, adopts a centre of mass (CoM) lumped model, meaning that the dynamics is computed on some points (the CoM) representative of the whole mass, through a Lagrangian approach, i.e. an approach where the computational grid moves together with the sliding mass.

The sliding mass is split into different blocks along the motion direction, obtaining a sort of a “chain” of interacting blocks, whose CoM movement is computed numerically. This “block” approximation allows one to follow accurately the fall of the mass and the consequent shape changes, simplifying significantly the motion equations: at each time step the acceleration, velocity and displacement of each block are calculated in the order, as well as its geometry (namely the block boundaries) and consistently the geometry of the entire slide, providing all data necessary to pass to the subsequent time step. As regards the block acceleration, it is given by the sum of the following contributions:

- the main acceleration term, comprehending the body forces (gravity and buoyancy, in case of underwater slides) and the bottom friction resistance resulting from the mass-sliding surface contact;
- the resistance term, accounting for all the interactions between the exposed mass surfaces (frontal and lateral) and the ambient;

- the internal interaction term, providing the reciprocal pushes between the blocks and controlling their lengthening or shrinking.

In order to adopt such approach, the code UBO-BLOCK1 needs as input the initial sliding mass and the undisturbed sliding surface: in our model the volume of the landslide is conserved, there is not deposition during the motion nor sliding surface erosion and volume increase. Also the pre-defined CoM trajectory has to be provided to the code, together with the lateral boundaries controlling the mass spreading.

It is worth mentioning that the code UBO-BLOCK1, further details of which can be found in TINTI *et alii* (1997), is a module of a more complex set of codes to investigate landslide-generated tsunamis and has been successfully applied to several case-studies, such as the Stromboli 2002 landslide tsunamis (TINTI *et alii*, 2006; TINTI *et alii*, 2008); the Stromboli Holocene landslide (TINTI *et alii*, 2000; TINTI *et alii*, 2003); the evaluation of the effects of the speculative tsunami induced by the Ischia Debris Avalanche (TINTI *et alii*, 2011); the investigation on the source of the 1693 eastern Sicily tsunami (TINTI *et alii*, 2012); the evaluation of the tsunamigenic potential of the North Gorringe Avalanche - Atlantic Ocean (Lo IACONO *et alii*, 2012).

DATA ELABORATION: THE SLIDING SURFACE AND THE INITIAL MASS MORPHOLOGY

In order to run the numerical simulation of the Vajont landslide, an accurate reconstruction of the sliding surface and of the sliding mass is needed. The large amount of data available both before and after the event allowed us to reconstruct the morphology of the sliding surface and of the collapsing body. Hereafter we outline the most significant steps of this procedure, starting with the digitalization of two maps containing the pre- and post-slide topography of the Vajont valley (DI SOPRA, 1997).

THE SLIDING SURFACE

One of the most striking features of the Vajont slide case is that in the upper part of the slope, more precisely on the western side, the slide left exposed well-defined clay layers that can be then easily considered the upper portion of the sliding surface, and that can be further assumed to constitute the sliding surface also in the part that remained covered under the

final deposit. Stratigraphic analyses carried out also on the unaffected slope around the detachment niche show that clay layers along Mt. Toc flank exhibit a 40°-45° slope angle in the upper part, and are found to be almost horizontal downslope in the valley bottom.

As can be deduced from Fig. 1 the run-out distance of the Vajont slide is rather limited and the final deposit is largely superimposed to the initial body. Accordingly, the sliding surface can be subdivided into three main areas:

- the upper portion, that is uncovered now, and hence coincides with the post-event topography;
- the lower surface that was initially exposed and downslope the slide toe and that resulted to be covered by the final mass deposit. Therefore this can be obtained from the pre-slide topography;
- the intermediate part covered by the depletion mass (as defined in WP/WLI 1993).

For this last portion of sliding surface some assumptions were made by HENDRON & PATTON (1985), basing on previous geological studies from ROSSI & SEMENZA (1965) and on profiles prior drawn by SELLI & TREVISAN (1964): the western side of the rupture surface supposedly follows a chair-like profile, steeper upslope and very low-angle downslope (see profiles 1-4 in Fig. 7), while the eastern side is conjectured to exhibit a parabolic trend (profiles 5-6 in the same Figure). The pre-existing clay layers, well visible in the upper part of the sliding surface, deepens eastward: SELLI & TREVISAN (1964) supposed that the sliding motion provoked the cut, in the downslope part of the eastern sliding surface, of calcareous rocks overlaying the clay, creating a new rupture surface with a higher friction coefficient, providing then the explanation for the observed slight eastward rotation experienced by the mass during sliding (HENDRON & PATTON, 1985). The lithological heterogeneity of the sliding surface has implications on the basal friction coefficients of the two sides as will be seen later.

In virtue of the above considerations and taking advantage from the along-slope profiles drawn SELLI & TREVISAN (1964) and by HENDRON & PATTON (1985), we reconstructed and digitized eight south-north transects, using them as the basis to obtain the intermediate unknown part through an interpolation procedure. Together with the other two parts obtained digitising the post- and pre-slide maps, this provided eventually a regular grid representing the topography of the entire sliding surface.

THE SLIDING BODY AND THE FINAL DEPOSIT

After reconstructing the complete sliding surface, obtaining the initial thickness of sliding body is a trivial matter since it is simply given as the point-to-point difference between the initial topography (pre-slide map) and the topography of the sliding surface.

Likewise, the thickness of the final deposit is by definition the difference between post-slide topography and the sliding surface.

By the procedure summarised here above we have been able to obtain a total volume of around $258.8 \times 10^6 \text{ m}^3$ for the initial slide, that is a value compatible with the estimates found in the literature. The final deposit turns out to be of a slightly lower volume, namely $248.5 \times 10^6 \text{ m}^3$. The lack of mass can be probably explained as the consequence of a second minor slide affecting the eastern lobe of the mass, occurring at the end of the main event according to HENDRON & PATTON (1985). Since in our model the slide conserves the volume, this discrepancy will affect the final simulated deposit.

In Fig. 2 the pre- and post-slide thicknesses are graphed: the transects are taken longitudinally (1 and 2) and transversally (3 and 4) with respect to the mass motion direction, mainly south-north oriented. Some features are evident: the mass concentrates more towards the slide front, as is visible in profiles 1 and 2 where the final deposit (red line) seems to be shorter

and higher than the initial one (green line) and more asymmetric, with the peak closer to the front. The transversal profiles 3 and 4 are taken respectively on the rear and on the frontal part of the initial and final deposits and are designated as 3pre, 4pre and as 3post and 4post in Fig. 2. What appears with evidence is that the sliding body, starting from a two-lobes mass distribution (profile 3pre, green line) compacts while moving downslope, showing a mass concentration on the eastern side (profile 3post red line). In the front, the initial body still presents a double lobe, though less prominent (profile 4pre, green line), while at the end of the motion one sees that the mass concentrates in the central part, reaching more than 270 m thickness. These features confirm what has been found in the literature: the mass concentration in the central part of the front in the valley bottom and a slight eastward rotation of the mass, probably being connected with the different behaviour of the rupture surface.

SLIDE STRIPPING

The input data of the slide evolution code UBO-BLOCK1 are the initial sliding mass and the sliding surface, that have been obtained as specified in the previous sections, and in addition the common trajectory of the block CoM and the lateral boundaries of the surface within which the slide is “channelled” (see TINTI *et alii*, 1997).

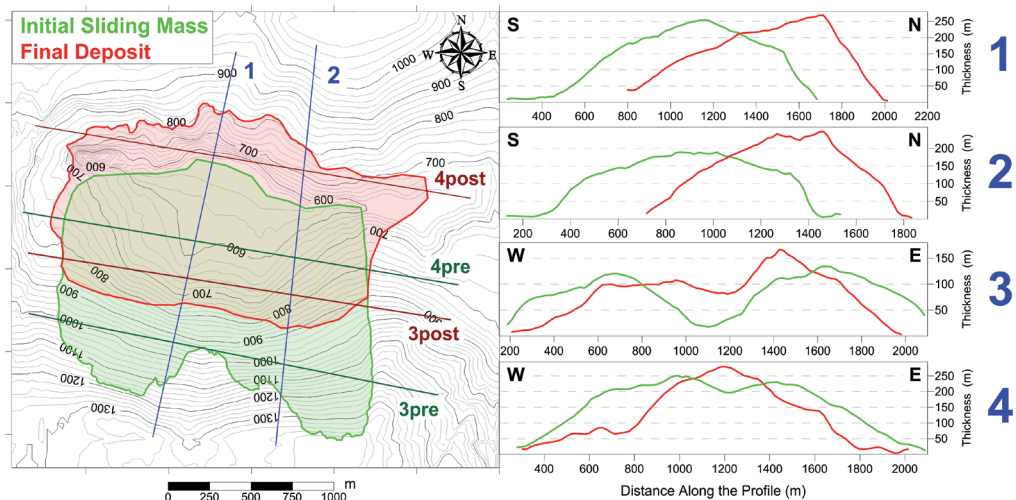


Fig. 2 - Reconstruction of the initial (green) and final (red) slide body, starting from the obtained sliding surface. The 1-4 lines marks the positions of the slices reported on the right panels, accounting for longitudinal transects (1 and 2) and transversal (3-4) ones with respect to the sliding motion (south-north). The 3 and 4 lines are taken along the rear and frontal parts of the pre- (green) and post-slide (red) body, and then respectively compared

The Vajont slide shows a considerable width (~1850 m) compared to the longitudinal extension (~400 m), while the model we adopt suits more “chain”-like slides, where the aspect ratio (length over width) is greater than 1. Using a single central path for the CoM would represent a too crude approximation, because this would imply neglecting the heterogeneity of the sliding surface.

In order to cope with the Vajont landslide lateral extension, we decided to split the landslide into different parallel strips, applying on each of them the UBO-BLOCK1 code and running them independently each other. Each “chain”-like sub-slide simulation needs its own sliding surface, initial sliding mass, CoM path and lateral boundaries, and also a final deposit thickness used as a constraint for the tuning of the model parameters. The subdivision was realized by trying to conserve the volume inside each strip, and accounting also for the slight easterly rotation already mentioned. Strips are shown in the first panel of Fig. 5. Most of the volume is included in strips 2 to 5, and here the percentage differences between the pre- and post-slide volumes are not more than 3% in each strip. The side strips show larger discrepancies. The westernmost strip, close to the Vajont dam, no. 1, involving only about 6% of the total volume, shows a slightly larger percentage difference (about 4%). But the eastern strip, no. 6, which includes 15% of the volume, has a deviation of about 29% of less volume which is mainly due to the already mentioned secondary slide, taking place after the main occurrence and bringing mass out of the computational boundaries.

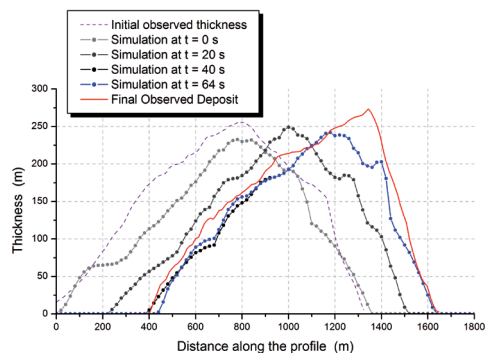


Fig. 3 - Slide thickness taken at different times for sub-slide 3, compared with the observed initial (purple dashed line) and final (red line) thickness. Values are computed along the CoM trajectory. Curves corresponding to 40 and 64 s are almost totally superimposed

RESULTS OF THE NUMERICAL SIMULATION

EXAMPLE OF SIMULATION: SUB-SLIDE 3

The slide motion was computed separately in each strip by means of the code UBO-BLOCK1. Each sub-slide was partitioned into a “chain” of 10 blocks, with approximately equal volume.

Figures 3 and 4 show some results of the landslide simulation for strip 3 with friction coefficient value $\mu = 0.14$, and more precisely the mass profile evolution and block velocities respectively.

We can notice that the sub-slide maintains its compactness, tending further to concentrate towards the front and to slightly shorten from the initial length of around 1300 m down to approximately 1200 m (Fig. 3). This is confirmed also by the quasi uniformity of the velocity of the individual blocks (black dots in Fig. 4), with differences smaller the 3-4 m/s at any time. The maximum velocity attained is 18 m/s after almost 20 seconds as concerns the average value (red line in Fig. 4), while some blocks approach 20 m/s.

The motion mainly stops after about 35 s, after which only one block still moves, though quite slowly. This is the first (uppermost) block of the chain, as visible also from Fig. 3, where one can appreciate that the $t=40$ s (black) profile almost coincides with the final one ($t=64$ s, blue dotted line), apart from a small difference in the rear part. It is worth remarking that the final simulated profile shows a very good approximation with the observed one. A quantitative way to measure the discrepancy between the final computed and ob-

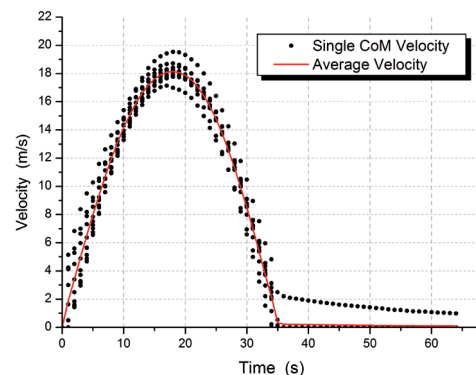


Fig. 4 - Velocity of the blocks CoM (black dots) and average velocity (red line) vs. time for sub-slide 3. Notice that after 35 s only one block is still moving, though slowly, while the velocity of the other CoMs is zero

served deposits is the misfit index, ranging from 0-1 and measuring the degree of lack-of-overlapping between to mass distributions (see ZANIBONI & TINTI, 2013; for further details). In this case the computed misfit index is 0.058, which means that the two distributions deviate from one another by less than 6%, or, alternatively, that they overlap by more than 94%.

SENSITIVITY ANALYSIS THROUGH THE FRICTION COEFFICIENT

By varying the bottom friction coefficients in each strip one can obtain different final sub-slide deposits and different speed curves. In playing with the value of μ within the reasonable range 0.10-0.40 we noticed that the results for the side strips 1 and 6 (see Fig. 5 for their position) were always the least satisfactory, which has induced us to neglect them in the rest

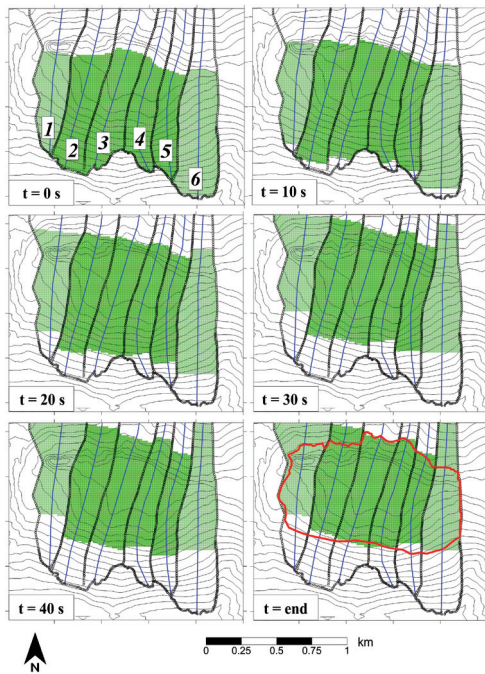


Fig. 5 - Calculated footprints of the six sub-slides shown at different times superimposed to the sliding surface topography. Strips are numbered from 1 to 6 starting from the westernmost strip (top left panel). Strips are separated by black lines. The blue lines within each strip are the CoM pre-defined trajectories, that are required as input data by the landslide simulation code UBO-BLOCK1. The central strips, involved in our sensitivity analysis, are marked in green, while the lateral ones, 1 and 6, are light green. The red line in the final map (bottom right) delimits the final deposit

of the analysis and to focus on the central strips accounting for the largest portion of the slide volume (about 80%). We noticed further that sub-slides tend to remain compact during the motion as occurs in the exemplary case of strip 3 with $\mu = 0.14$ given in the previous section, since individual blocks tend to move with similar speed at any time. Therefore, the time-history of the average speed (red line in Fig. 4) can be taken as representative of the velocity of all blocks.

In performing our analysis we consider three basic issues:

- 1) The first is that the final deposit poses a severe constraint to the simulation, so that the goal is the minimisation of the misfit, i.e. the achievement of the maximum overlapping between the simulated deposit and the observed one in the strips considered.
- 2) The second key point is that, in consequence of the evidence that the whole Vajont slide remained compact during the motion, differential velocities between the different sub-slides are hard to accept. Therefore the second goal to attain is the minimisation of deviations between the curves of the average speeds of the various sub-slides. It is worth observing here that to measure the deviation among speed curves, one exploits the same quantitative misfit used for the volume distribution but with two main differences: in this case the objects to compare are curves instead of surfaces and second they are in number of four (corresponding to the velocity curves of sub-slides 2-5) instead of two.
- 3) The third item is that since the bottom friction coefficients are essentially determined by the properties of the rocks that are in contact and that the western side of the sliding surface (including strips 2-4) is different from the eastern side (strip 5), hence we assume the same friction coefficient for the set of sub-slides 2-4 and a possible different friction coefficient for the other sub-slide, no. 5.

An immediate observation is that satisfying the first two items above is impossible because searching for the least deposit misfit was found to lead to discrepant velocities and vice versa, minimising the velocity misfit resulted to lead to an unsatisfactory deposit misfit. The most appropriate strategy to follow therefore seems to be to search for a compromise, where none of the two indices are minimised but rather a combination of the two. Indeed it is simple to define a global misfit index that is weighted average of the deposit and velocity

misfit (see ZANIBONI & TINTI, 2013, for further details).

The result of the minimisation process described here is that the best global misfit has the value of 0.106, corresponding to a velocity misfit of 0.091 and a deposit misfit of 0.129, and this is achieved when the friction coefficient used for the west-side sub-slides 2-4 is $\mu_w = 0.14$ and that for the east-side sub-slide 5 is $\mu_e = 0.27$. With this parameter setting, the Vajont slide, seen as the composition of the six sub-slides, moves as is depicted in Fig. 5, where the footprints of each sub-slide at different times are portrayed (in green). For the side strips no 1 and no 6 we used respectively the west- and the east-side value of the friction coefficients, i.e. $\mu_w = 0.14$ and $\mu_e = 0.27$. Since the results of these simulations were not taken into account in the global misfit minimisation procedure, they are marked distinctly in light green. Our attention concentrates on the central strips 2-5, showing a satisfactory homogeneity during the sliding motion and presenting an almost compact front moving northward, downslope, with only strip 4 moving slightly ahead of the others. After $t = 30$ s the slide picture seems not to change significantly, and the $t = 40$ and $t = \text{fin}$ views are practically coincident. The final (bottom right) panel of Fig. 5 shows also the boundary of the Vajont slide deposit, depleted however of the mass involved in the secondary eastward slide (compare it with the one given in Fig. 2). The agreement between observed and computed boundaries is very satisfactory in the central strips, while in lateral strips is quite bad since they both lengthen too much and go well beyond the observed front.

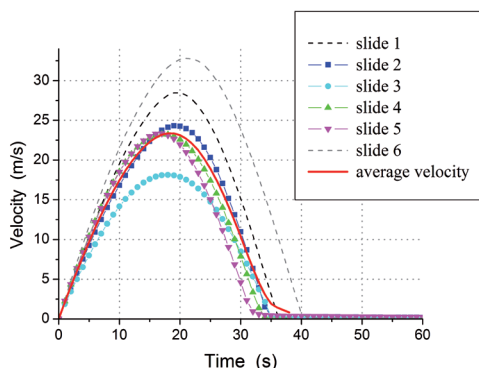


Fig. 6 - Average velocities of the six sub-slides vs. time, for the case $\mu_w=0.14$ and $\mu_e=0.27$. The curves for sub-slides 1 and 6, plotted with black and grey dashed lines, did not enter the misfit minimisation procedure, but are reported for the sake of completeness

The velocity plot of Fig. 6 confirms that slides in strips 1 and 6 move quite different from the others with higher speed and longer motion. Restricting to the central core of the slide, we observe that sub-slides 2, 4 and 5 go rather coherent with similar speed curves, but sub-slide 3 moves slower than the other and is the one that most contributes to the value of the velocity misfit. The average velocity (red line) goes up to 23 m/s at about $t = 20$ s, fully compatible with the findings by SELLI & TREVISAN (1964), suggesting 20 m/s, and later by SEMENZA (2002), increasing the value to 20-25 m/s. The whole slide motion, in addition, seems to last 35-40 seconds, slightly shorter than the value of 40-50 s estimated by SELLI & TREVISAN (1964) and CALOI (1966) studying seismic records.

To complete the picture of the final results, cross-sections of the slides taken along the CoM trajectories (see their location in Fig. 5) are given in Fig. 7. Here, for each strip, the profile of the sliding surface forms the basis above which the initial profile of the slide as well as the computed and the observed deposits are shown. In general a good agreement can be noticed between the observed deposit (light grey) and the final position of the simulated slide (blue line). Notice also that in the simulation the mass mainly deposits in the bottom of the valley and only partially climbs up the northern opposite flank, reaching farther than the real slide. This occurs for example for strip 2 and slightly for strip 5. This is evident also for the side strip 1 and much more for the side strip 6 and was already mentioned in commenting the maps of Fig 5.

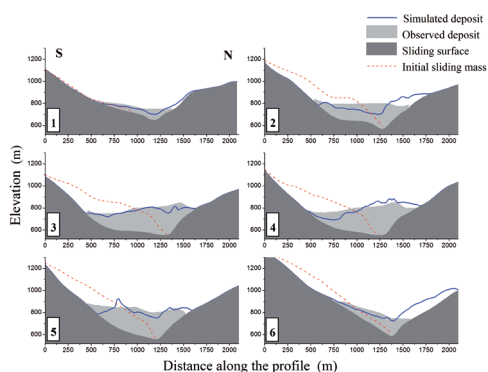


Fig. 7 - Cross-sections for the six strips, with the sliding surface marked in grey. The initial thickness is represented by a dashed red line, the simulated deposit by a blue line. The observed deposit is shown in light grey

The final remark regards the sliding surface. From the cross-sections it appears clear that on the southern flank (left on the figure) profiles 1-4 (on the west of the slide) exhibit a sharp change of gradient from steep to mild around mid-slope, while profiles 5 and 6 (on the east) do not: this is the consequence of the hypothesis we adopted in reconstructing the sliding surface as described in a previous section: chair-like shape profiles for the clay layer located on the west and parabolic shape for the calcareous rock rupture surface one finds on the east.

DISCUSSION AND CONCLUDING REMARKS

In this paper we have carried out the numerical simulation of the Vajont landslide by using a code UBO-BLOCK1 implementing a block Lagrangian model. The features of the slide that were relevant for the simulations are:

- 1) clay layers remained exposed uphill on the west side of the detachment niche;
- 2) mass deposit compactness with preserved layer sequences, which suggests the existence of a well-defined sliding surface;
- 3) the mass deformed as the effect of the slide, somewhat shortening and concentrating toward the centre of the front;
- 4) a slight eastward rotation of the sliding mass;
- 5) the slide moved fast reaching peak speed around 20-25 m/s, and lasted around 40-50 s, which suggests small values for the bottom friction coefficient, lower than the usual one for clay surfaces.

The numerical code used for simulations represents the sliding body as a chain of contiguous blocks, preserving mass and able to deform. Needed inputs for the code are the sliding surface, the initial geometry of the slide, the lateral boundaries of the area swept by the slide, and the common path of the CoM of the blocks forming the slide. Relevant outputs are the position, velocity and acceleration of all the block CoMs vs. time, and, in addition, the basal area and height of each block. From all of this, the shape of the entire slide is known as a function of time and in particular the computed final shape can be compared with the observed deposit.

Great attention was devoted to reconstructing the sliding surface. The uphill and downhill parts of the surface were derived by making use of pre- and post-slide topographic maps, while the intermediate

part was built on the hypothesis (advanced by HENDERON & PATTON, 1985) of a “chair”-like downslope profile for the western side and of a parabolic shape for the eastern part, basing also on SELLI & TREVISAN (1964) transects. The initial geometry of the slide and the final deposit were straightforward products of the sliding surface reconstruction, and turned out to be of almost similar volumes ($260 \times 10^6 \text{ m}^3$ vs. $250 \times 10^6 \text{ m}^3$), the small deficit being explainable by invoking a secondary slide evacuating some mass after the main slide occurrence. Volume matching found a posteriori is in support of the correctness, or at least strong plausibility, of the reconstructed surface of sliding.

Stripping of the slide into six sub-slides with length predominant over width was made to meet the class of application for which the numerical code UBO-BLOCK1 was conceived. Strips were defined in such a way that they intercept similar volume in the initial slide body and in final deposit. In our simulations the six sub-slices move independent from one other.

The most important parameter in the model is the bottom friction coefficient, influencing the velocity of the blocks, the duration of the motion and the run-out distance. Differences between the west- and east-side of the sliding surface induced us to use two values for this coefficient, one for the western strips 1-4, where supposedly the bottom surface is clay and another for the eastern strips 5-6, where instead it is characterized by a calcareous rock component. The bulk of the analysis was however performed only on the central strips 2-5 involving 80% of the total volume, neglecting the side strips 1 and 6.

The main slide features we have chosen to relate are the position and geometry of the final deposit and the fact that the slide moved with the same velocity as a unique body, though our modelling implies that it is the ensemble of independent sub-slides. Fitting both items turned out to be a conflicting issue, and hence it was opted for a combined minimization of discrepancies. These were measured by introducing a quantitative index of misfit measuring the similarity of distributions. For the deposit, a deposit misfit index was defined measuring the difference between the computed and observed distributions of mass for the set of sub-slides 2-5. Further for the velocity, the slide velocity curves of these sub-slides were compared in pairs and a total velocity misfit was then obtained as an average. Eventually, the deposit and the velocity in-

dices were combined together to get the global misfit.

The result was that the friction coefficients leading to the smallest global misfit are very different from one another, $\mu_w = 0.14$ for the western side of the sliding surface, and $\mu_e = 0.27$ for the eastern. The slide simulated by using these parameters showed a satisfactory agreement with the observed final deposit (see Figs. 5 and 7). Moreover, the average speed of the whole slide, obtained as the weighted mean of the individual sub-slide speeds, was consistent with estimates given in the literature. The mass reaches 23 m/s in about 20 s and in the next 15 s it decelerates (see Fig. 6), and reaches the valley bottom, showing a compact front moving northward (see Fig. 5). The total duration of the slide motion is about 35 s, slightly smaller than the one deduced in the literature from the analysis of seismic records. Further, the sub-slides move with similar velocities, but sub-slide 3 has a speed always somewhat smaller than the others, which is unsatisfactory.

The main results of our analysis is that assuming a different geometry of the sliding surface, one in the west-side (chair-like profile) and another on the east side (parabolic profile), implies that the friction coefficients must be very different, and much smaller on the west-side. This may have some geological explanation in the lithological difference of the sliding surface, consisting respectively of clay layer and of calcareous rocks. Going further with this hypothesis,

a scenario can be imagined where the failure started on the west involving the contact of the mass with the clay layer and then propagated eastward where rupture passed across different layers.

This analysis needs refinement and probably code improvements. Using a fully 2D landslide simulation code accounting for lateral interaction between adjacent blocks (in terms of the present discretisation, this would involve interaction between adjacent sub-slides) will lead to a coherent movement of the whole slide in a natural way, without the need of making recourse to the speed misfit index. Further, in our model all sub-slides move only in one direction, and are not allowed to reverse their motion. Some authors however claimed that evidence was found that the Vajont mass, after climbing up the opposite flank, returned back to the bottom of the valley (e.g. SEMENZA & GHIROTTI, 2000), which would imply a longer duration of the motion and a longer slide path, and, consequently, smaller friction coefficients.

What our simplified modelling proved is the strict association between the two-shape geometry of the sliding surface and the two-value friction coefficient. Though more sophisticated models can expectedly lead to some correction to these values, we are confident that this chief feature will be maintained. Confirmation or falsification of this findings demands for more specific geological investigations on the properties of the rock material involved in the sliding process.

REFERENCES

- ARGNANI A., ARMIGLIATO A., PAGNONI G., ZANIBONI F., TINTI S. & BONAZZI C. (2012) - *Active tectonics along the submarine slope of south-eastern Sicily and the source of the 11 January 1693 earthquake and tsunami*. Nat. Hazards Earth Syst. Sci., **12**: 1311-1319, doi:10.5194/nhess-12-1311-2012.
- BOSA S. & PETTI M. (2011) - *Shallow water numerical model of the wave generated by the Vajont landslide*. Environmental Modelling & Software, **26**: 406-418.
- CALOI P. (1966) - *L'evento del Vajont nei suoi aspetti geodinamici*. Annali di Geofisica, **XIX**: 1-74 (in Italian).
- CARLONI G.C. & MAZZANTI R. (1964) - *Rilevamento geologico della frana del Vajont*. Giornale di Geologia, Annali del Museo Geologico di Bologna, **XXXII**: 105-123 (in Italian).
- CECINATO F., ZERVOS A. & VEVEAKIS E. (2011) - *A thermo-mechanical model for the catastrophic collapse of large landslides*. Int. J. Numer. Anal. Meth. Geomech., **35**: 1507-1535.
- CIABATTI M. (1964) - *La dinamica della frana del Vajont*. Giornale di Geologia, Annali del Museo Geologico di Bologna, **XXXII**: 139-153 (in Italian).
- DI SOPRA L. (1997) - *Valle del Vajont, situazione pre-impatto. Settembre 1963 - scala 1:5000 and Valle del Vajont, situazione post-impatto. Novembre 1963 - scala 1:5000*. Studio Di Sopra, Udine.
- GHIROTTI M. (1994) - *Modellazione numerica della frana del Vajont sulla base di nuovi dati*. Geologica Romana, **30**: 207-216 (in Italian).
- HENDRON A.J. & PATTON F.D. (1985) - *The Vajont slide, a geotechnical analysis based on new geological observations of the failure surface*. Technical report GL85-5, US Army Corps of Engineers Waterways Experiment Station, Vicksburg, (2 volumes).

- LO IACONO C., GRACIA E., ZANIBONI F., PAGNONI G., TINTI S., BARTOLOME R., MASSON D., WYNN R., LOURENCO N., PINTO DE ABREU M., DAÑOBEITIA J.J. & ZITELLINI N. (2012) - *Large and deep slope failures in the Gorringe Bank: evidence for landslide-generated tsunamis along the SW Iberian Margin*. *Geology*, **40**: 931-934. doi: 10.1130/G33446.1.
- MÜLLER L. (1964) - *The rock slide in the Vajont Valley*. *Rock Mechanics and Engineering Geology*, **2**: 148-212.
- MÜLLER L. (1968) - *New considerations on the Vajont slide*. *Rock Mechanics and Engineering Geology*, **6**: 1-91.
- PANIZZO A., DE GIROLAMO P., DI RISIO M., MAISTRI A. & PETACCIA A. (2005) - *Great landslide events in Italian artificial reservoirs*. *Natural Hazards and Earth System Sciences*, **5**: 733-740.
- PAPARO M.A., ZANIBONI F. & TINTI S. (2013) - *The Vajont landslide, 9th October 1963: Limit equilibrium model for slope stability analysis through the minimum lithostatic deviation method*. In this volume.
- ROSSI D. & SEMENZA E. (1965) - *Carte geologiche del versante settentrionale del Monte Toc e zone limitrofe, prima e dopo il fenomeno di scivolamento del 9 ottobre 1963*. Istituto di Geologia dell'Università di Ferrara. Scale 1:5000; 2 maps, colored.
- SELLI R. & TREVISAN L. (1964) - *Caratteri e interpretazioni della frana del Vajont*. *Giornale di Geologia, Annali del Museo Geologico di Bologna*, **XXXII**: 7-68 (in Italian).
- SEMEZA E. & GHIROTTI M. (1998) - *Vajont-Longarone 34 anni dopo la catastrofe*. *Annali dell'Università di Ferrara (Nuova serie), sezione Scienze della Terra*, **7**: 73-94 (in Italian).
- SEMEZA E. & GHIROTTI M. (2000) - *History of the 1963 Vajont slide: the importance of geological factors*. *Bulletin of Engineering Geology and the Environment*, **59**: 87-97.
- TIKA T.H.E. & HUTCHINSON J.N. (1999) - *Ring shear tests on soil from the Vajont landslide slip surface*. *Geotechnique*, **49**: 59-74.
- TINTI S., BORTOLUCCI E. & VANNINI C. (1997) - *A block-based theoretical model suited to gravitational sliding*. *Natural Hazards*, **16**: 1-28.
- TINTI S., BORTOLUCCI E. & ROMAGNOLI C. (2000) - *Computer simulations of tsunamis due to flank collapse at Stromboli, Italy*. *Journal of Volcanology and Geothermal Research*, **6**: 103-128.
- TINTI S., PAGNONI G., ZANIBONI F. & BORTOLUCCI E. (2003) - *Tsunami generation in Stromboli Island and impact on the south-east Tyrrhenian coasts*. *Natural Hazards and Earth System Sciences*, **3**: 299-309.
- TINTI S. & ZANIBONI F. (2004) - *Lagrangian 1D and 2D models for the simulation of the Vajont landslide, October 9th, 1963, Italy*. 32nd International Geological Congress, Florence, Italy, 20-28 August 2004, abstract and poster n. 103-25.
- TINTI S., PAGNONI G. & ZANIBONI F. (2006) - *The landslides and tsunamis of 30th December 2002 in Stromboli analysed through numerical simulations*. *Bull. Volcanol.*, **68**: 462-479.
- TINTI S., ZANIBONI F., PAGNONI G. & MANUCCI A. (2008) - *Stromboli island (Italy): scenarios of tsunamis generated by submarine landslides*. *Pure Appl. Geophys.*, **165**: 2143-2167.
- TINTI S., CHIOCCI F.L., ZANIBONI F., PAGNONI G. & DE ALTERIIS G. (2011) - *Numerical simulation of the tsunami generated by a past catastrophic landslide on the volcanic island of Ischia, Italy*. *Mar. Geophys. Res.*, **32**: 287-297.
- VARDOULAKIS I. (2002) - *Dynamic thermo-poro-mechanical analysis of catastrophic landslides*. *Geotechnique*, **52**: 157-171.
- WARD S. & DAY S. (2011) - *The 1963 landslide and flood at Vajont reservoir, Italy. A tsunami ball simulation*. *Ital. J. Geosci.*, **130**: 16-26.
- WP/WLI - UNESCO WORKING PARTY FOR WORLD LANDSLIDE INVENTORY (1993) - *Multilingual Landslide Glossary*. The Canadian Geotechnical Society.
- ZANIBONI F. (2004) - *Modelli numerici di evoluzioni di frane con applicazione a casi di frane tsunamigeniche subaeree e sottomarine*. PhD. Thesis, XVI Cycle, Department of Earth Sciences, University of Bologna (in Italian).
- ZANIBONI F. & TINTI S. (2013) - *Numerical simulations of the 1963 Vajont Landslide, Italy: application of 1D lagrangian modelling*. *Natural Hazard*, under revision, July 2013.